MODELLING, SIMULATION AND EXPERIMENTAL VERIFICATION OF A 3 DOF MOVING PLATFORM WITH PARALLEL KINEMATICS AND ELECTRO-HYDRAULIC PROPORTIONAL / SERVO CONTROL SYSTEM

Ezz Eldin Ibrahim*, Ahmed Azouz, Tarek Elnady, Mohamed Saffaa Hassan, Ibrahim Saleh

Military Technical College, Cairo, Egypt

*E-mail of corresponding author: ezzbos@gmail.com

Ezz Eldin Ibrahim 0000-0001-9377-7852,
Tarek Elnady 0000-0003-1060-1742,
Ahmed Azouz 0000-0002-7697-6611,
Mohamed Saffaa Hassan 0000-0002-8557-9706

Resume

Hydraulic motion platforms are widely utilized in various environments due to their capacity to bear heavy loads and provide long actuator strokes. The predominant control system employed for hydraulic motion platforms is the electro-hydraulic servo system (EHSS) due to its high accuracy and robustness. However, compared to other types of hydraulic valves, the electro-hydraulic servo valve (EHSV) is less durable. An alternative system to EHSS is the electro-hydraulic proportional system (EHPS), which employs an electro-hydraulic proportional valve (EHPV) instead of the EHSV. The EHPV resolves the durability issue at the expense of accuracy and system error. The optimization of durability and accuracy is the core of this study. The tracking behavior and response of both Three degrees of freedom (3 DOF) motion platforms using EHSS and EHPS are investigated across different frequency ranges.

Article info

Received 15 May 2024
Accepted 11 September 2024
Online 7 October 2024

Keywords:

hydraulic valve
electro-proportional valve
servo valve
electro-hydraulic proportional system
electro-hydraulic servo system
position tracking control
motion platform

Available online: https://doi.org/10.26552/com.C.2025.001

ISSN 1335-4205 (print version)
ISSN 2585-7878 (online version)

1 Introduction

Motion platforms are devices comprising two platforms, with the lower platform being stationary while the upper platform follows the desired motion. They are widely used in transportation simulators, replicating real-world vehicle movements with high precision. They enhance driver training, vehicle testing, and the development of advanced driving assistance systems. Numerous research works have focused on electro-hydraulic systems, exploring their various aspects. Akers et al. [1] extensively discussed the potential configurations of electro-hydraulic systems, providing insights into the performance analysis of system components and operational methodologies. Additionally, Watton [2] delved into the modelling and simulation of electro-hydraulic systems, exploring mathematical derivations of different hydraulic system structures.

Electro-hydraulic systems have gained significant popularity in numerous industrial applications due to their exceptional capacity to deliver high torque and force while maintaining a favorable power-to-weight ratio. These Hydraulic Servo Systems find applications across a wide range of industries, including aircraft, robotics, mining machinery, manufacturing systems, active suspensions, test machines, paper machines, and injection molding machines.

The primary objective of an electro-hydraulic system is to precisely control the desired displacement. To achieve this goal, advanced techniques have been developed to ensure high response and minimize errors. Typically, displacement control and error reduction involve comparing the position, velocity, pressure, and force of the system's output against the input signal, thereby striving to achieve the desired response as accurately as possible.

Optimal system tuning has been extensively explored by researchers, who have employed various methodologies to achieve the desired results. These include root locus analysis, and the Zeigler-Nichols method [3] that are the most famous techniques

used in this field. Genetic Algorithm (GA), Particle Swarm Optimization (PSO), and Adaptive Weighted PSO (AWPSO) are examples of evolutionary techniques that are used for tuning Proportional, Integral, and Derivative (PID) controller. The PID controller is applied in this approach to hydraulic servo system (HSS) simulation model and real-time HSS.

Electro-hydraulic servo systems EHSS have been studied by many researchers due to their great importance in industrial fields. One of the main problems in studying EHSS is the nonlinearity problem of the dynamics of the hydraulic system as stated by Sohl et al. [4]. The friction, non-smooth motion, and valve directional change resulted in system nonlinearities. Many studies dealt with analyzing and controlling the nonlinearity of EHSS. These studies helped in providing system stability for a good position and force tracking.

To ensure accurate tracking of position, acceleration, pressure, and force, the EHSS has been equipped with various automatic controllers. Guan and Pan [5] presented a new control technique based on an adaptive sliding mode method for controlling the electro-hydraulic system. The controlling method is applied experimentally, and the results proved the effectiveness of it in tracking any trajectory by the hydraulic actuator. Niksefat and Sepehri [6-7] used a quantitative feedback theory (QFT) to control the hydraulic actuator displacement by evaluating the force acting on the cylinder. Lichen et al. [8] presented a new control strategy for hydraulic servo systems to obtain more robustness and stability using the PID tuning.

Tian [9] studied the actuator external torque and invented a new control theory. The utilization of a Fuzzy Logic Controller (FLC) has been highlighted for precise position control of electro-hydraulic actuators. Additionally, an (ACO) ant colony optimization technique is employed to optimize the parameters of the fuzzy neural network, ensuring the attainment of optimal values [10].

The enhancement of position-tracking performance is achieved through the application of the invariance principle and feed-forward compensation, utilizing the pole-zero placement theory of the system. This approach allows for the development of improved control strategies to ensure accurate and efficient position tracking, as described in [11].

A hydraulic position servo system control is established by employing a Particle Swarm Optimization (PSO) algorithm to regulate the PID loops. This implementation enables effective optimization of the control parameters, resulting in improved performance and precision of the servo system as presented in [12]. The force control of the hydraulic servo system is achieved through the design and implementation of fuzzy controllers. These controllers are specifically designed to minimize force overshoot and protect the load from potential failure. By employing the fuzzy control techniques, the system ensures precise force regulation and safeguards the overall stability and integrity of the load, as illustrated in [13]. Three control strategies are employed to regulate an electro-pneumatic 3DOF platform by Prieto et al. [14].

Proportional valves demand significantly higher input power typically hundreds of milliamps or more compared to servo valves, which operate on mere tens of milliamps as mentioned by Bin [15]. While proportional valves offer less precise control and can exhibit greater hysteresis, the servo valves excel in accuracy. The performance of EHSV is discussed by MI et al. [16].

In the previous review, focused on controlling stabilization platforms and electro-hydraulic systems, the emphasis was placed on selecting an appropriate control method to address system errors and transient response. However, this study shifts its attention to the key control component of the hydraulic system, namely the electro-hydraulic valve. It delves into examining the impact of valve parameters on platform stability and the potential for improving error reduction within the system.

2 Model description

The 3 DOF motion platform shown in Figure 1 consists of the lower plate, which is fixed, and the upper plate which is moving to track the required position. The two plates are connected via three hydraulic actuators driven by an electro-hydraulic system. The actuators are joined with the two plats by six universal joints. The electro-hydraulic system forces the three actuators to extract or retract to enable the upper plate to track the required motion. The figure shows the orientation of the three axes x, y, and z and two rotations which are roll and pitch.

The overall system of the 3 DOF motion platform is depicted in the block diagram shown in Figure 2. The input signal from the transition motion in the z-direction and the rotation motion in both roll and pitch were transformed to a linear motion by the mean of the rotation matrix block, which are described later. These signals were then analyzed after feeding back from the position sensor and operating the EHSVs/ EHPVs. The three valves were fed by the required flow rate from the hydraulic power block. The three actuators are operated to drive the upper plate with the required input position signal. The lower plate remained stationary as a reference frame, so the motion of the upper plate was referred to concerning it.

3 Modeling of 3 DOF motion platform using EHPS and EHSS

The electro-hydraulic system could be used for motion platforms; it can be either EHSS or EHPS. The mathematical model of the EHPS for one hydraulic

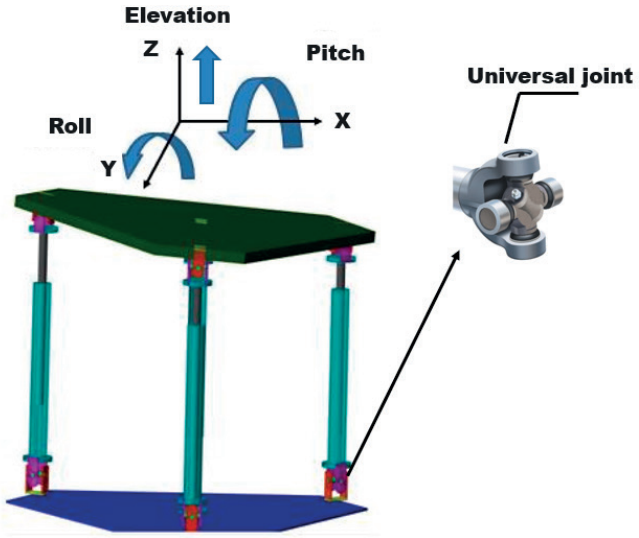

Figure 1 *Motion platform with 3 DOF motion*

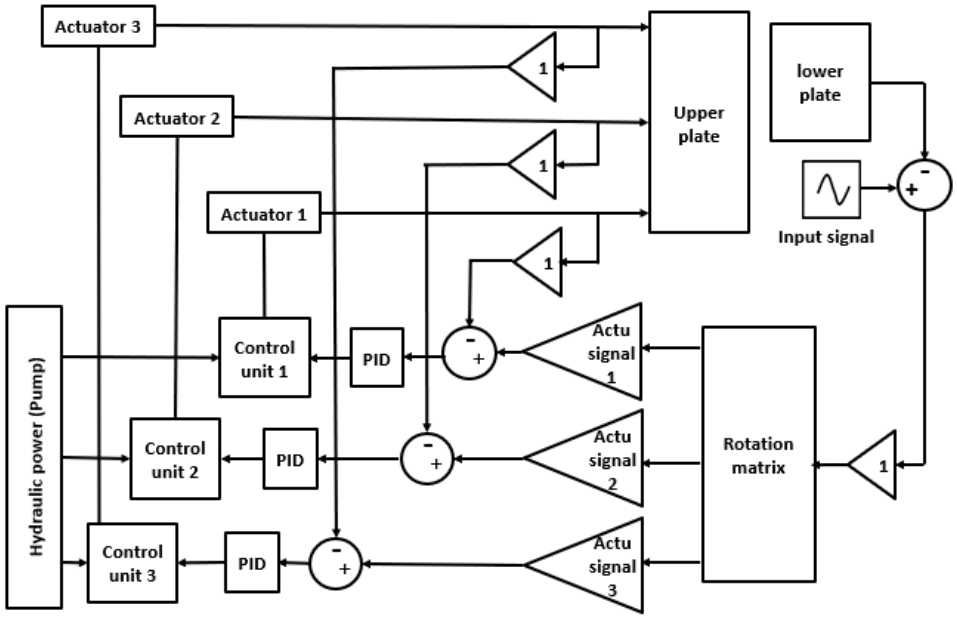

Figure 2 *Hydraulic motion platform with 3 DOF block diagram*

actuator was discussed recently by Yuan in [17] and [18]. The mathematical model is derived in this section. The single hydraulic actuator system is then integrated into the MATLAB Simulink program to model the 3 DOF motion platform. The Q-P mathematical relation of the pump was found in Rabie [19], as follows:

$$Q_P = Q_{th} - cP_G\,, \tag{1}$$

where:
Q_{th} is the theoretical maximum flow rate of the gear pump,
c is a constant equal $7\text{x}10^{-3}$,
P_G is the pump output pressure.

The mathematical equations, which describe the operation of the relief valve, as in Rabie [19], are:

The equation of poppet motion:

$$m_p \frac{d^2z}{dt^2} + f_r \frac{dz}{dt} + k_r(z + z_0) = pA_p + F_{seat} \tag{2}$$

$$F_{seat} = K_r z_0\,, \tag{3}$$

$$A_p = \pi D^2/4(m^2)\,, \tag{4}$$

where:
m_p is the relief valve poppet mass, kg,
z is the displacement of relief valve poppet, m,
f_r is the pump output pressure,
K_r is the stiffness coefficient of relief valve spring, N/m,
A_p is the poppet area of the relief valve, m^2,

F_{seat} is the seat reaction of the relief valve, N.

The flow-rate equation through the relief valve is:

$$Q_{rv} = C_d A_p \sqrt{\frac{2(P - P_t)}{\rho}}, \quad (5)$$

where:
C_d is the discharge coefficient.
P_t is the tank pressure, Pa.

The EHPV is a 4/3 valve hydraulic ring manufactured of type NG6. It is designed with a valve spool that exhibits zero overlap and is regulated by the movement of two electrical proportional solenoids.

The equation of motion of the valve spool could be written as follows:

$$F_s = m_s \frac{d^2x}{dt^2} + f_s \frac{dx}{dt} + k_s x, \quad (6)$$

where:
m_s is the mass of spool (kg),
f_s is the EHPV spool damping coefficient [13] (N),
k_s is the EHPV return spring stiffness (N/m),
x is the spool displacement.

The first term on the right-hand side of Equation (6) represents the inertia force of the spool during motion. The second term represents the damping force, while the last term represents the force applied by the return spring. The internal orifices of the valve are shown in Figure 3.

The flow-rate equations throughout the valve orifices are given by the following equations:
from port B to port T,

$$Q_a = C_d A_a(x) \sqrt{\frac{2(P_B - P_t)}{\rho}}, \quad (7)$$

from port P to port B,

$$Q_b = C_d A_b(x) \sqrt{\frac{2(P_s - P_B)}{\rho}}, \quad (8)$$

from port P to port A,

$$Q_c = C_d A_c(x) \sqrt{\frac{2(P_s - P_A)}{\rho}}, \quad (9)$$

from port A to port T,

$$Q_d = C_d A_d(x) \sqrt{\frac{2(P_A - P_t)}{\rho}}, \quad (10)$$

where:

$$A_a = A_c = A_r \qquad x \geq 0, \quad (11)$$

$$A_b = A_d = \omega \sqrt{(x^2 + c^2)} \qquad x \geq 0, \quad (12)$$

$$A_a = A_c = \omega \sqrt{(x^2 + c^2)} \qquad x \leq 0, \quad (13)$$

$$A_b = A_d = A_r \qquad x \geq 0, \quad (14)$$

where
ω is the width of the port,
c is the spool radial clearance,
x is the valve opening distance,
A_r is the radial clearance area.

To obtain a mathematical model for the cylinder; the internal and external flows of the cylinder are described in the schematic drawing shown in Figure 4.

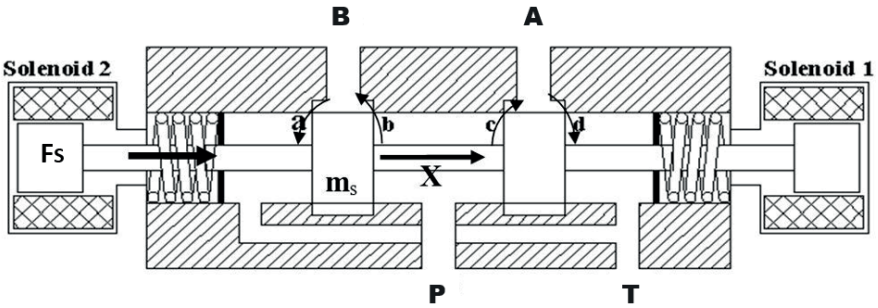

Figure 3 *Internal orifices of proportional-directional valve*

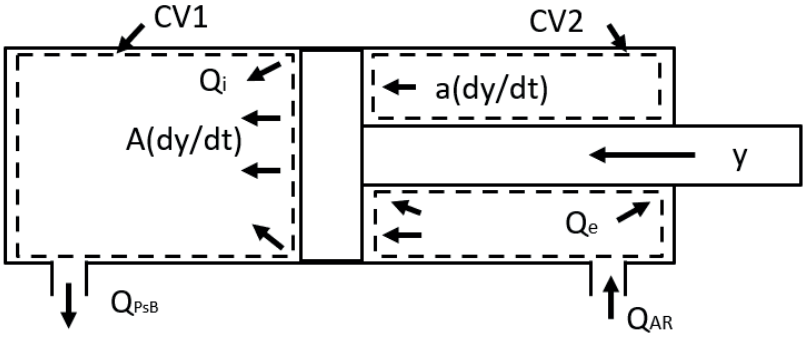

Figure 4 *Flow directions inside and outside the hydraulic cylinder*

The continuity equation, applied on the control volume CV1and CV2, could be written as follows:

$$Q_{AR} - a\frac{dy}{dt} - Q_i - Q_e - \frac{(V_R + ay)}{B} \times \frac{dP_R}{dt} = 0\,, \quad (15)$$

$$A\frac{dy}{dt} - Q_i - Q_{PsB} - \frac{(V_{PS} + Ay)}{B} \times \frac{dP_{Ps}}{dt} = 0\,. \quad (16)$$

The equation of motion, applied for the piston and its rod, could be described as follows:

$$aP_R - AP_{Ps} = m_c\frac{d^2y}{dt^2} + f_c\frac{dy}{dt} + F\,. \quad (17)$$

4 Analysis for kinematics

Much research dealt with the 6DOF parallel manipulator platform and its motion. This study focuses on investigating the design and implementation of a system that incorporates inverse kinematics and motion monitoring for a 3DOF platform. The aim is to explore the execution and effectiveness of this system as done by [20]. The system enables motion along is the three linear translations (x, y, and z directions) and three rotations around the three axes (yaw, pitch, and roll, denoted as ψ, θ, and ϕ, respectively).

In this study, 3 DOF is the main concern which are two rotation pitch θ, roll ϕ, and one translation in the z-direction. These linear and rotation motions are represented in Figure 5, by representing the two frames; one is fixed while the other is moving with respect to the fixed frame. The length vector between the fixed and a moving plate l is determined from the following equation:

$$l_{i} = \mathbf{t} + \mathbf{P_i} \cdot \mathbf{R_P} - \mathbf{b_i} \quad (18)$$

where:
l_i is the length of the actuators,
t is the translational position vector of the origin of the moving frame with respect to the reference frame,
$\mathbf{P_i}$ are represents each actuator's position vector about the moving frame,
$\mathbf{b_i}$ are represents each actuator's position vector about the reference frame,
$\mathbf{R_p}$ are represents a mix of rotation matrix stationary and moving frames by knowing input rotation angles in roll and pitch, as discussed in [13].

$$\mathbf{R_p} = \begin{bmatrix} C_\theta & 0 & S_\theta \\ S_\theta S_\phi & C_\phi & -C_\theta S_\phi \\ -S_\theta C_\phi & S_\phi & C_\theta C_\phi \end{bmatrix}, \quad (19)$$

where:
C_θ is cos θ and S_ϕ is sin ϕ, etc.

The design of a 3DOF translational parallel manipulator, utilizing hydraulic actuation, was recently studied by [21].

The mathematical model of the entire hydraulic system could be obtained by integrating all derived mathematical equations with the aim of the MATLAB Simulink program. The system transfer function was identified using the system identification tool as follows:

$$f(s) = \frac{8.468S + 11.05}{S^2 + 8.522S + 11.11}\,. \quad (20)$$

Modelling and validation of the EHSV system are done based on the published work by Ibrahim et al. [22]. The model was utilized in this study to simulate the 3 DOF motion platform using the MATLAB Simulink program.

5 Experimental work

The 3 DOF motion platform test rig was established with EHPS using The Military Technical College laboratory facilities. The test rig was used to investigate the motion of the platform in roll and pitch directions with a maximum inclination angle of 10° and elevation up to 100 mm.

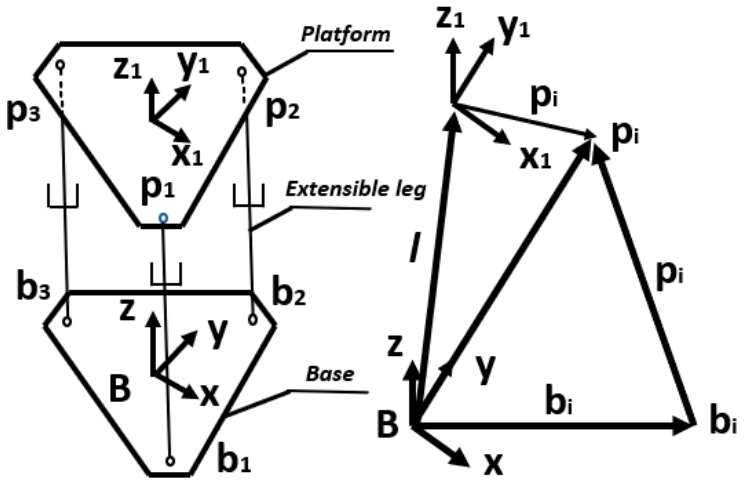

Figure 5 *Coordinates diagram for 3 DOF motion platform*

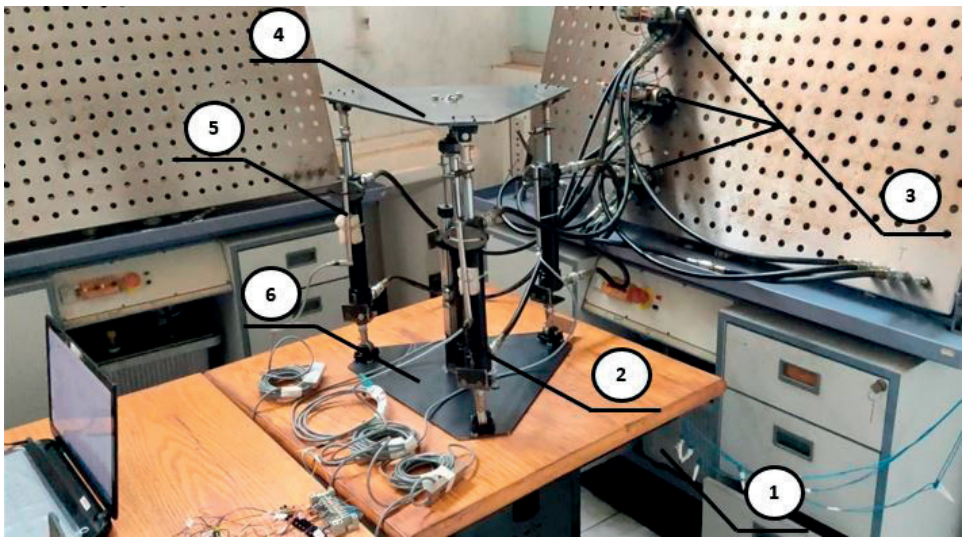

Figure 6 *Experimental test rig for 3DOF hydraulic motion platform*

Table 1 *Hydraulic circuit components description*

Component	Specification
Pump	A fixed displacement gear pump produces up to 6.05 liters per minute at its highest output flow rate, at a nominal speed of 600 rpm
RV.	Relieving pressure at 60 bar
PV.	4/3 EHPV type NG6
Actuator	Cylinder to road ratio 1.6:1 with 32/22 mm area and a max. pressure of 160 bar

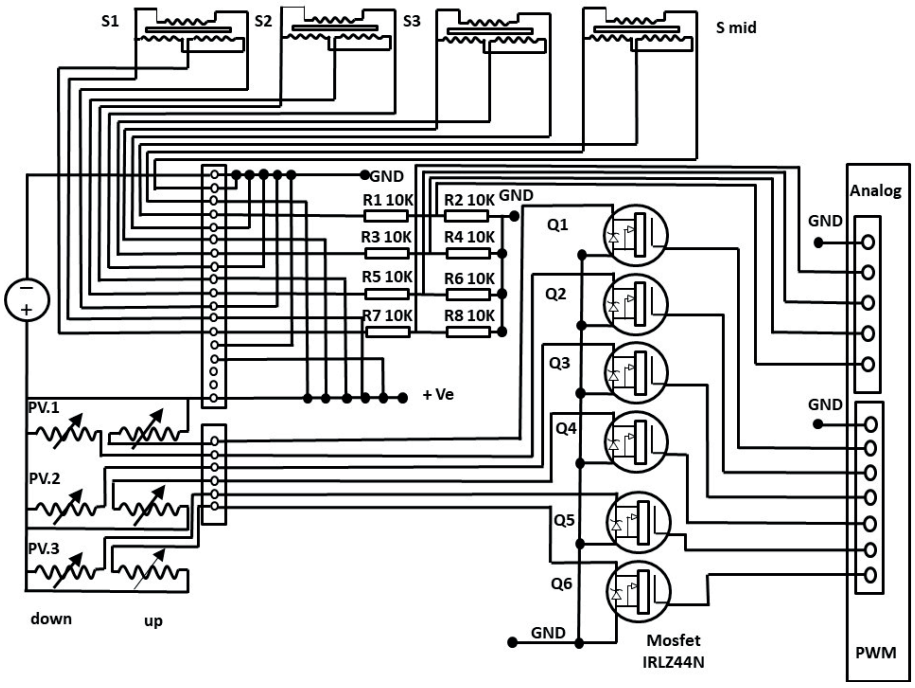

Figure 7 *Electric circuit for controlling 3 DOF hydraulic stabilization platform*

Figure 6 shows the test rig which consists of an oil tank (1) that delivers the circuit with the required hydraulic oil. Three hydraulic actuators (2) were used to perform the required motion by the feeding from three (EHPV) (3), which are the main control unit. Two plates (4) and (6) are used as upper and lower plates, respectively. Three (LVDT) (5) are used to feed the controller with the cylinder's displacement. The hydraulic circuit components are described in Table 1.

The electric circuit used in controlling the proposed motion platform is designed with the aid of the "Proteus 8.8" program [23]. Figure 7 illustrates the block diagram

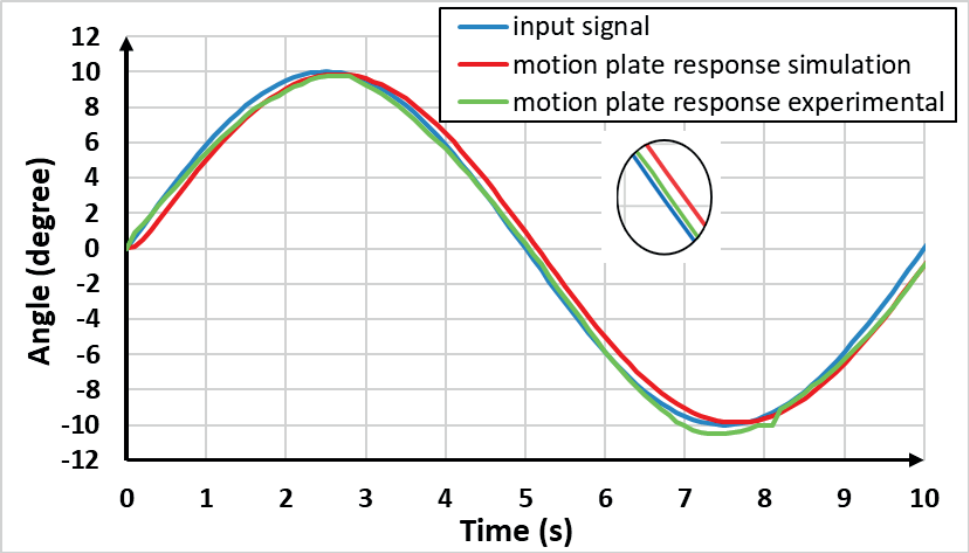

Figure 8 *Experimental and model tracking the behavior of 3DOF motion platform with EHPS to a roll motion*

of this electric circuit. Four LVDT sensors are used in this circuit using a power supply of 24 V DC and its output signal is 10 V DC. The control card is Arduino Mega with input/output volt 5 V DC. Two 10-ohm resistors are used in series to protect the control card from damage. Arduino delivers the sensors signal to the MATLAB Simulink program to adjust the required output to the proportional valve coils. The output voltage of the control card is 5 V DC while the proportional valve coils operate at 24 V DC. Thus, to increase the pulse width modulation from a voltage range of ±5 V DC to ±24 V DC, six MOSFET transistors (IRLZ44) are utilized.

6 System validation

The 3DOF motion plate in this study utilizes an electro-hydraulic proportional valve EHPV instead of EHSV. The outcomes of tracking the motion platform's behavior (experimental vs. model), in response to a sinusoidal input signal with a 10° amplitude and 0.1 Hz frequency, are displayed in Figure 8. When compared to the input signal and the experimental findings, the model shows a good tracking position. There was a recorded 0.038 root-mean-square error between the motion platform model and the input signal. However, there was a 0.046 root-mean-square error between the experimental and model results. The model has a good tracking position with the input signal. The maximum motion platform model tracking angle recorded ±9.86° (i.e., it deviates from its maximum target by 0.14°).

7 Result and discussion

The motion platforms with EHSS and EHPS are examined by applying a sinusoidal input signal with a frequency range (0.1 - 0.5 Hz) to study their tracking behavior. Figure 9 shows the tracking behavior of the motion platform with both systems EHSS and EHPS to a sinusoidal input signal with an amplitude of 10° and frequency of 0.1 Hz. The two models have a good tracking position with the input signal. The root-mean-square error between the input signal and the motion platform with EHPS was recorded at 0.038 and the maximum motion platform tracking angle was recorded at ±9.86° (i.e., it deviates from its maximum target by 0.14°). The root-mean-square error between the input signal and the motion platform with EHSS was recorded at 0.02 and the maximum motion platform tracking angle was recorded at ±9.9° (i.e., it deviates from its maximum target by 0.1°).

Figure 10 shows the motion platform response with EHSS and EHPS to a sinusoidal wave with a frequency of 0.5 Hz and amplitude of 10°. The motion platform with EHPS tracks the input signal with a root-mean-square error of 0.27 and the maximum motion platform tracking angle recorded ±8.67° (i.e., it deviates from its maximum target by 1.33°). The motion platform with EHSS tracks the input signal with a root-mean-square error of 0.11 and the maximum motion platform tracking angle recorded ±9.6° (i.e., it deviates from its maximum target by 0.4°), which agreed with the data plotted in [24].

Figure 11 shows a comparison between the 3DOF motion platform with EHSS and EHPS by applying the input-signal frequencies (0.1, 0.2, 0.3, 0.4, and 0.5 Hz). The results focus on deviation from the maximum target angle. The results show that both systems are affected by high frequency. The results, shown in Figure 12, represent the recorded root-mean-square error with respect to the input signals. Both system's error increases by increasing the input-signal frequency. However, the error resulting from using the EHPS has a major record in comparison to EHSS.

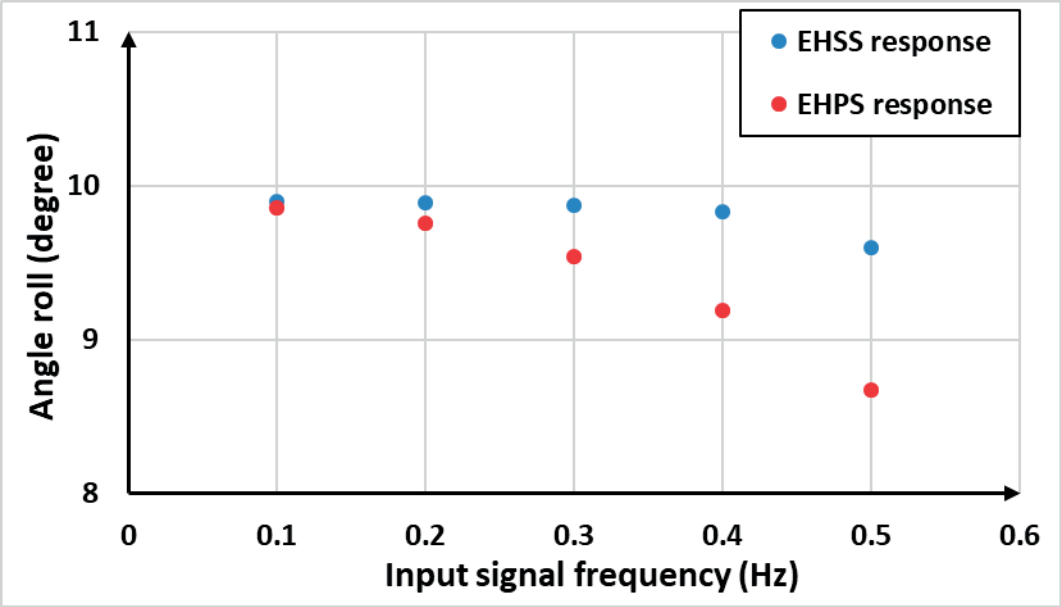

Figure 11 Deviation of the 3 DOF motion platform from the maximum target using EHSS and EHPS

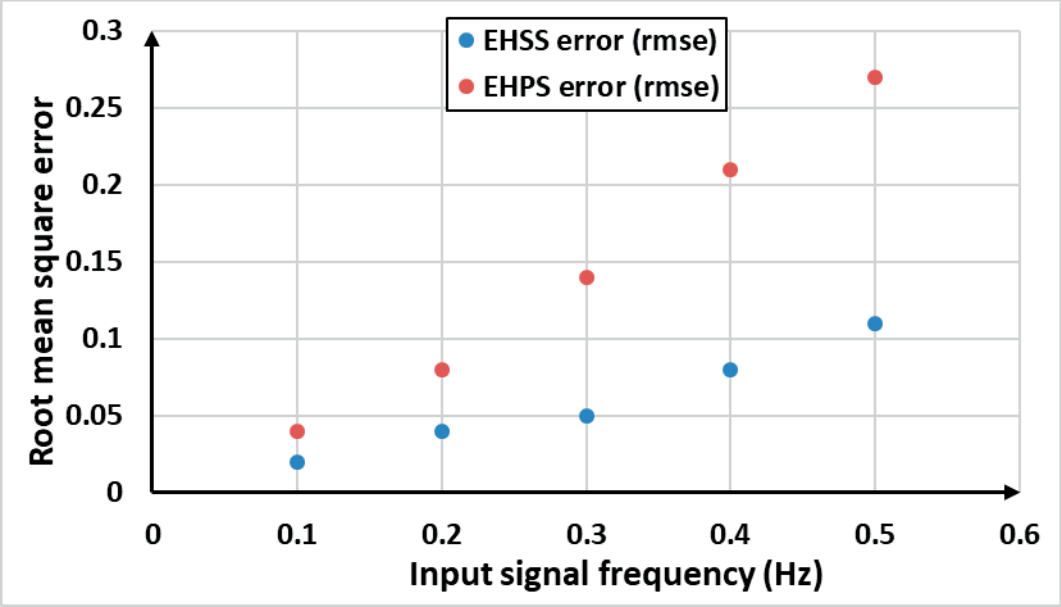

Figure 12 *Root-mean-square error of the 3DOF motion platform using EHSS and EHPS*

Table 2 *EHSS and EHPS tracking behavior by changing input signal frequency*

Input frequency (Hz)	RMSE between the model and input EHSS.	RMSE between the model and input EHPS.	Deviation from target EHSS	Deviation from target EHPS
0.1	0.02	0.038	0.1°	0.14°
0.2	0.04	0.08	0.11°	0.24°
0.3	0.05	0.14	0.13°	0.46°
0.4	0.08	0.21	0.17°	0.81°
0.5	0.11	0.27	0.4°	1.33°

Figure 12 shows the effect of changing the input signal frequency on the platform stability and the deviation achieved from the accurate required inclination using EHSS and EHPS, which is also clarified in Table 2. The platform deviates from its target as the frequency is increased by using both systems; however, by using the EHPS the deviation is larger than by using EHSS. These results confirm the effectiveness of EHPS in

low-frequency applications and it is not useful for high frequency up to 0.3 Hz.

8 Conclusion

This study was focused on the design and analysis of 3DOF motion plate models equipped with EHPS and EHSS to investigate their respective frequency ranges.

Firstly, both motion platforms were evaluated, and it was observed that their responses were nearly identical for the low-frequency input signals. This suggests that both systems are capable of effectively handling low-frequency motions.

However, as the input signal frequency increased, both systems exhibited an increase in error. Notably, the EHPS system demonstrated a significant error compared to the EHSS system. This indicates that the EHSS system outperforms the EHPS system in terms of accuracy and precision, especially at higher frequencies.

The suggested motion platform with EHPS, which has been extensively tested and verified over a wide range of frequency ranges, is the best suited for the low-frequency applications, according to the study's findings. This platform can be employed in scenarios where precise motion control is required within a relatively lower frequency range.

In summary, this research contributes to understanding of the frequency capabilities and limitations of the 3DOF motion plate models with EHPS and EHSS. The results highlight the superior performance of the EHSS system, particularly at higher frequencies, while emphasizing the suitability of the EHPS system for the low-frequency applications. These findings can inform the selection and utilization of motion platforms in diverse industrial and research settings. Further research can focus on optimizing the performance of EHPS systems to mitigate their error at higher frequencies and enhance their overall functionality.

Acknowledgment

The authors received no financial support for the research, authorship and/or publication of this article.

Conflicts of interest

The authors declare that they have no known competing financial interests or personal relationships that could have appeared to influence the work reported in this paper.

Reference

[1] AKERS, A., GASSMAN, M., SMITH, R. *Hydraulic power system analysis* [online]. 1. ed. Boca Raton: CRC Press, 2006. eISBN 9780429191176. Available from: https://doi.org/10.1201/9781420014587

[2] WATTON, J. *Fluid power systems: modeling, simulation, analog and microcomputer control*. Prentice-Hall, Inc., 1989. ISBN 978-0133231977.

[3] PUANGDOWNREONG, D., SUKULIN, A. Obtaining an optimum PID controllers for unstable systems using current search. *International Journal of Systems Engineering, Applications and Development*. 2012, **6**(2), p. 188-195. eISSN 2074-1308.

[4] SOHL, G. A., BOBROW, J. E. Experiments and simulations on the nonlinear control of a hydraulic servosystem. *IEEE Transactions on Control Systems Technology* [online]. 1999, **7**(2), p. 238-247. ISSN 1063-6536, eISSN 1558-0865. Available from: https://doi.org/10.1109/87.748150

[5] GUAN, C., PAN, S. Adaptive sliding mode control of electro-hydraulic system with nonlinear unknown parameters. *Control Engineering Practice* [online]. 2008, **16**(11), p. 1275-1284. ISSN 0967-0661, eISSN 1873-6939. Available from: https://doi.org/10.1016/J.CONENGPRAC.2008.02.002

[6] NIKSEFAT, N., SEPEHRI, N. Designing robust force control of hydraulic actuators despite system and environmental uncertainties. *IEEE Control Systems Magazine* [online]. 2001, **21**(2), p. 66-77. ISSN 1066-033X, eISSN 1941-000X. Available from: https://doi.org/10.1109/37.918266

[7] NIKSEFAT, N., SEPEHRI, N. Design and experimental evaluation of a robust force controller for an electro-hydraulic actuator via quantitative feedback theory. *Control Engineering Practice* [online]. 2000, **8**(12), p. 1335-1345. ISSN 0967-0661, eISSN 1873-6939. Available from: https://doi.org/10.1016/S0967-0661(00)00075-7

[8] YU, M., LICHEN, G. Fuzzy immune PID control of hydraulic system based on PSO algorithm. *Telkomnika Indonesian Journal of Electrical Engineering* [online]. 2013, **11**(2), p. 890-895. ISSN 1693-6930, eISSN 2302-9293. Available from: https://doi.org/10.11591/TELKOMNIKA.V11I2.2048

[9] TIAN, J. Study on control strategy of electro-hydraulic servo loading system. *Telkomnika Indonesian Journal of Electrical Engineering* [online]. 2013, **11**(9), p. 5044-5047. ISSN 1693-6930, eISSN 2302-9293. Available from: https://doi.org/10.11591/TELKOMNIKA.V11I9.3246

[10] ROZALI, S. M., RAHMAT, M. F., HUSAIN, A. R., KAMARUDIN, M. N. Design of adaptive backstepping with gravitational search algorithm for nonlinear system. *Journal of Theoretical and Applied Information Technology*. 2014, **59**(2), p. 460-468. ISSN 1992-8645, eISSN 1817-3195.

[11] YAO, J.-J., DI, D.-T., JIANG, G.-L., LIU, S. High precision position control of electro-hydraulic servo system based on feed-forward compensation. *Research Journal of Applied Sciences, Engineering and Technology*. 2012, **4**(4), p. 289-298. ISSN 2040-7459, eISSN 2040-7467.

[12] ROOZBAHANI, H., WU, H., HANDROOS, H. Real-time simulation based robust adaptive control of hydraulic servo system. In: 2011 IEEE International Conference on Mechatronics ICM 2011: proceedings [online]. IEEE. 2011. ISBN 978-1-61284-982-9, eISBN 978-1-61284-985-0, p. 779-784. Available from: https://doi.org/10.1109/ICMECH.2011.5971220

[13] CHEN, H. M., SHEN, C. S., LEE, T. E. Implementation of precision force control for an electro-hydraulic servo press system. In: 2013 3rd International Conference on Intelligent System Design and Engineering Applications ISDEA 2013: proceedings [online]. IEEE. 2013. ISBN 978-1-4673-4893-5, p. 854-857. Available from: https://doi.org/10.1109/ISDEA.2012.202

[14] RUBIO, E., PRIETO, P. J., HERNANDEZ, L., URQUIJO, O. Comparison between three control strategy applied to an electro-pneumatic 3-DOF platform. In: IEEE CHILEAN Conference on Electrical, Electronics Engineering, Information and Communication Technologies CHILECON 2019: proceedings [online]. IEEE. 2019. eISBN 978-1-7281-3185-6. Available from: https://doi.org/10.1109/CHILECON47746.2019.8986866

[15] YU, B. ET AL., Design, mathematical modeling and force control for electro-hydraulic servo system with pump-valve compound drive. *IEEE Access* [online]. 2020, **8**, p. 171988-172005. eISSN 2169-3536. Available from: https://doi.org/10.1109/ACCESS.2020.3012091

[16] MI, J., YU, J., HUANG, G. Direct-drive electro-hydraulic servo valve performance characteristics prediction based on big data and neural networks. *Sensors* [online]. 2023, **23**(16), 7211. eISSN 1424-8220. Available from: https://doi.org/10.3390/S23167211

[17] YUAN, X. J., LING, H. T., CHEN, J. J., FENG, Y., QIU, T. Y., ZHAO, R. CH. A dynamic modelling method for an electro-hydraulic proportional valve combining multi-systems and moving meshes. *Journal of the Brazilian Society of Mechanical Sciences and Engineering* [online]. 2022, **44**(7), p. 1-13. ISSN 1678-5878, eISSN 1806-3691. Available from: https://doi.org/10.1007/s40430-022-03603-x

[18] YUAN, X., SHI, S., WANG, C., WEI, L., LUO, C., CHEN, J. Dynamic modeling method for an electro-hydraulic proportional valve coupled mechanical-electrical-electromagnetic-fluid subsystems. *Journal of Magnetism and Magnetic Materials* [online]. 2023, **587**, 171312. ISSN 0304-8853, eISSN 1873-4766. Available from: https://doi.org/10.1016/J.JMMM.2023.171312

[19] RABIE, M. G. *Fluid power engineering*. New York: McGraw-Hill, 2009. ISBN 9780071626064.

[20] WEI, M. Y. Design and implementation of inverse kinematics and motion monitoring system for 6dof platform. *Applied Sciences* [online]. 2021, **11**(19), 9330. eISSN 2076-3417. Available from: https://doi.org/10.3390/app11199330

[21] DINDORF, R., WOS, P. Design of a hydraulically actuated 3-DoF translational parallel manipulator. *AIP Conference Proceedings* [online]. 2019, **2077**(1), p. 020015-1-020015-12. ISSN 0094-243X, eISSN 1551-7616. Available from: https://doi.org/10.1063/1.5091876

[22] IBRAHIM, E. E., ELNADY, T., HASSAN, M. S., SALEH, I. Modelling, transient response and hydraulic behaviour of 2DOF stabilization platform. *FME Transactions*. 2020, **48**(4), p. 833-840. ISSN 1451-2092, eISSN 2406-128X.

[23] PCB design and circuit simulator software - Proteus [online] Accessed: Aug. 16, 2024. Available from: https://www.labcenter.com

[24] RAD, S. A., TAMIZI, M. G., MIRFAKHAR, A., MASOULEH, M. T., KALHOR, A. Control of a two-DOF parallel robot with unknown parameters using a novel robust adaptive approach. *ISA Transactions* [online]. 2021, **117**, p. 70-84. ISSN 1879-2022, eISSN 0019-0578. Available from: https://doi.org/10.1016/J.ISATRA.2021.02.001

Appendix

Table A *Nomenclature*

Symbol	Definition
a	Cylinder area rod side, m^2
A	Cylinder area piston side, m^2
A_a	PV. Throttle area (a), m^2
A_b	PV. Throttle area (b), m^2
A_c	PV. Throttle area (c), m^2
A_d	PV. Throttle area (d), m^2
A_p	RV. Poppet area, m^2
B	Hydraulic oil's bulk modulus of elasticity, $N.m^{-2}$
C_d	Coefficient of discharge
C	Radial clearance, m
d	Cylinder rod side diameter, m
D	Cylinder side piston diameter, m
f_r	RV. Poppet damping coefficient, $N.sec.m^{-1}$
f_s	PV. Spool damping coefficient, $N.sec/m^{-1}$
F_s	PV. Solenoid force, N
F_{seat}	RV. Seat reaction, N
k	PV. Spring stiffness, $N.m^{-1}$
m_p	RV. Poppet mass, kg
m_s	PV. Moving parts mass, kg
p	Pressure, Pa
P_A	PV. Pressure port (A), Pa
P_B	PV. Pressure port (B), Pa
P_P	PV. Pressure port (P), Pa
P_t	Tank pressure, Pa
Q	Flow rate, m^3/sec
Q_a	PV. Flow rate through area (a), m^3/sec
Q_{AR}	Flow rate from port A to rod side chamber in the hydraulic cylinder, $m^3.sec^{-1}$
Q_b	PV. Flow rate through area (b), $m^3.sec^{-1}$
Q_c	PV. Flow rate through area (c), $m^3.sec^{-1}$
Q_d	PV. Flow rate through area (d), $m^3.sec^{-1}$
x	PV. Spool displacement, m
y	Displacement of the cylinder rod, m
z	RV. Poppet displacement, m